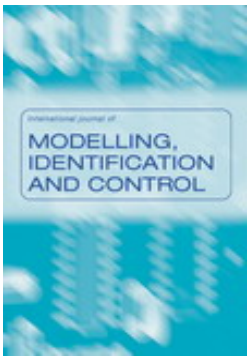

International Journal of Modelling, Identification and Control

ISSN online: 1746-6180 - ISSN print: 1746-6172
https://www.inderscience.com/ijmic

Analysis and control for ideal variable transmission ratio characteristics of active front wheel steering

Xiaojun He, Kun Yang, Yile Chang, Chao Ma, Wei Wang, Jie Wang

DOI: 10.1504/IJMIC.2024.10064195

Article History:

Received:	22 August 2023
Last revised:	23 January 2024
Accepted:	09 February 2024
Published online:	30 September 2024

Analysis and control for ideal variable transmission ratio characteristics of active front wheel steering

Xiaojun He

School of Transportation and Vehicle Engineering,
Shandong University of Technology,
Zibo, 255000, China
Email: lxjdeyouxiang9@163.com

Kun Yang*

School of Transportation and Vehicle Engineering,
Shandong University of Technology,
Zibo, 255000, China
Email: yangkun_sdut@163.com
*Corresponding author

Yile Chang

SAIC Motor R&D Innovation Headquarters,
Shanghai, 201800, China
Email: changyile_sdut@163.com

Chao Ma

School of Transportation and Vehicle Engineering,
Shandong University of Technology,
Zibo, 255000, China
Email: mc@sdut.edu.cn

Wei Wang

CATARC Automotive Test Center (Tianjin) Co., Ltd.,
Tianjin, 300300, China
Email: wangwei2011@catarc.ac.cn

Jie Wang

School of Transportation and Vehicle Engineering,
Shandong University of Technology,
Zibo, 255000, China
Email: wang-jie@sdut.edu.cn

Abstract: The change law of ideal transmission ratio with vehicle speed and hand-wheel angle is studied based on constant gain of steady-state vehicle system. It is used to resolve the conflict between steering sensitivity at the low-speed segment and steering stability at the high-speed segment for the traditional vehicle. For preventing the sudden change of hand-wheel torque caused by the transmission ratio change, the ideal variable transmission ratio (VTR) law is fitted by the improved S-type function and optimised by particle swarm optimisation (PSO) algorithm. For improving driving stability of vehicle, the stability control strategy based on linear quadratic regulator (LQR) is studied based on the optimised ideal variable transmission ratio control law. The front wheel angle is decided by the vehicle stability control strategy, and then the active front wheel steering (AFS) motor angle is obtained by the AFS calculation module to realise the AFS control. The closed-loop driver-vehicle system is established. This system includes driver model, the vehicle dynamic model, AFS model and so on. The results indicate that the performance of the proposed controller is good in the front wheel steering angle control for the better tracking to desired vehicle state.

Keywords: ideal variable transmission ratio; improved S-type function; particle swarm optimisation algorithm; linear quadratic regulator; LQR; active front wheel steering; AFS.

Reference to this paper should be made as follows: He, X., Yang, K., Chang, Y., Ma, C., Wang, W. and Wang, J. (2024) 'Analysis and control for ideal variable transmission ratio characteristics of active front wheel steering', *Int. J. Modelling, Identification and Control*, Vol. 45, No. 1, pp.40–57.

Biographical notes: Xiaojun He is currently a Master at the School of Transportation and Vehicle Engineering, Shandong University of Technology, Zibo, China. His research is focused on electric vehicles and vehicle dynamics control.

Kun Yang is currently a Professor at the School of Transportation and Vehicle Engineering, Shandong University of Technology, Zibo, China. He received his PhD degree from Jilin University. His research is focused on electric vehicles and vehicle dynamics control.

Yile Chang is currently an Engineer at the SAIC Motor R&D Innovation Headquarters, Shanghai, China. He graduated from Shandong University of Technology with a Master's degree. His research is focused on electric vehicles and vehicle dynamics control.

Chao Ma received his PhD in Mechanical Engineering from Sungkyunkwan University, Korea, in 2013. Since 2013, he is working as an Assistant Professor at Shandong University of Technology. His main research interests focuses on the design of powertrain system, control strategy for HEV, PHEV and EV.

Wei Wang is currently a Senior Engineer at CATARC Automotive Test Center (Tianjin) Co., Ltd. He received his PhD degree from Jilin University. His research is focused on new energy vehicles.

Jie Wang is currently an Associate Professor at the School of Transportation and Vehicle Engineering, Shandong University of Technology, Zibo, China. Her research is focused on 3S technology and intelligent transportation.

1 Introduction

In recent years, active front wheel steering (AFS) has been gradually applied in the field of automotive active safety. An additional angle independent of driver input can be applied to the steering wheels through an electric motor. This can achieve the variable transmission ratio (VTR) control for steering system to a certain extent. It can be used to resolve the conflict between steering sensitivity at the low-speed segment and steering stability at the high-speed segment for the traditional vehicle (Cho and Huh, 2019; Zhao et al., 2022). It is effective for improving the manoeuvrability, steering stability and trajectory keeping ability of the vehicle (Li et al., 2018; Zhang et al., 2022).

At present, the research on AFS mainly focuses on three aspects. They are the structure design of AFS, the AFS model and control algorithm based on ideal model, and integrated control for AFS and other chassis control systems. For the first aspect, Shimizu et al. (1999) designed a mechanical structure, and the VTR characteristics were realised by varying the amount of the offset between two shafts jointed at the tip of their arms. At the same time, the steering characteristics were analysed under high-speed steering and low-speed parking conditions. Wei et al. (2013) designed a new active steering system with the original electric power steering system. The driver's hand force was adjusted by the original power assist motor, and the AFS motor was used to output the additional angle independent of the driver. The active obstacle avoidance, lane keeping and yaw stability control were achieved by the new active steering system. For the second aspect, Kim et al. (2006) proposed an AFS system based on planetary gear mechanism with VTR. The transmission ratio was adjusted according to the vehicle speed, and vehicle stability was improved. Qi et al. (2021) established the AFS system model and seven-degree-of-freedom (7-DOF) model. The fuzzy control and sliding mode control for AFS are compared. The results show that the control effect of slide mode control is better in improving the stability of steering control. For the third aspect, the vehicle stability control was achieved by coordinated control of active rear steering (ARS) and differential braking when the differential braking system could not meet the requirement of stability control (Choi and Choi, 2016). Wu et al. (2022) proposed a coordinated control and an intervention method based on the working state of lateral tyre force for direct yaw control (DYC) and AFS system. The control effect is verified on low adhesion road surfaces. Pi et al. (2021) proposed a layered functional framework for the coordination of AFS and active stabiliser bar (ASB). The yaw and roll stability can be maintained and the contradiction of coupling control can be overcome based on actively adjusting the coordinated rules.

Figure 1 The research workflow (see online version for colours)

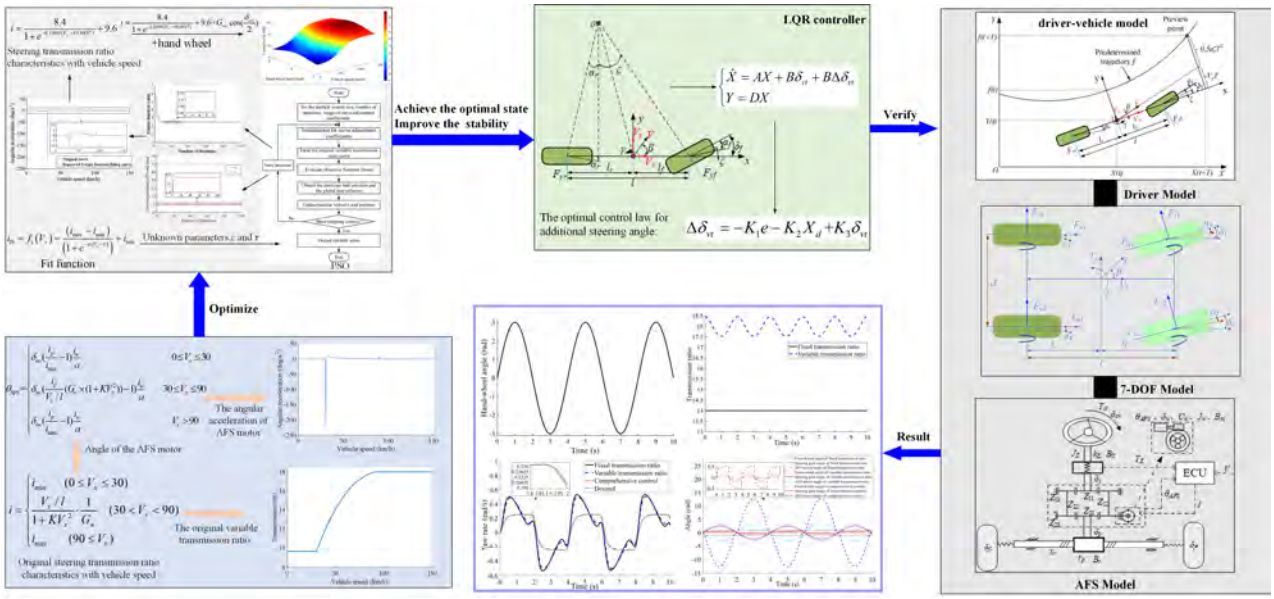

In conclusion, there has been some research on the optimisation of VTR law and AFS. However, there is relatively little research on the variation of AFS motor angle with vehicle speed by combining the law of VTR with AFS mechanical system. Based on previous studies, it is found that the conventional variable ratio law may cause an abrupt change in the angular acceleration of the AFS motor with the increase of vehicle speed. This will reduce the vehicle stability when turning. For that, the ideal VTR law optimised by the improved S-type function is analysed, and unknown parameters of the function are optimised by particle swarm optimisation (PSO) algorithm. The abrupt change in the angular acceleration of the AFS motor with vehicle speed is eliminated. Moreover, considering the deviation between the actual front wheel angle and the ideal front wheel angle, the vehicle stability control strategy based on linear quadratic regulator (LQR) is proposed to correct the preliminary AFS motor angle. A closed-loop driver-vehicle system is established for verifying the effectiveness of the optimised VTR law and the performance of the control strategy based on it.

2 Driver-vehicle system

For describing the research methodology more clearly, the schematic representation of the research workflow is shown in Figure 1. The defects of the original VTR law with vehicle speed are found, and it is the sudden change in the angular acceleration of the AFS motor with the vehicle speed. For solving the problem, the improved S-type function is used to fit variable original transmission ratio curve, and the PSO algorithm is applied to optimise its parameters. Considering the influence of the hand wheel (HW) on the transmission ratio, the new VTR rule is further constructed. For improving the steering stability and making the vehicle state to be close to the optimal value, the LQR controllers are studied. The driver-vehicle model is built to verified control strategies, and the verification is given in the last section.

2.1 Driver model

The driver model is applied to make the vehicle drive under the given operating conditions. The function of the driver module is to make the vehicle follow the predetermined trajectory. The optimal preview control theory is adopted to build the driver model based on fixed lateral acceleration (Ding et al., 2010). Its principle is shown in Figure 2.

Figure 2 The preview principle based on fixed lateral acceleration (see online version for colours)

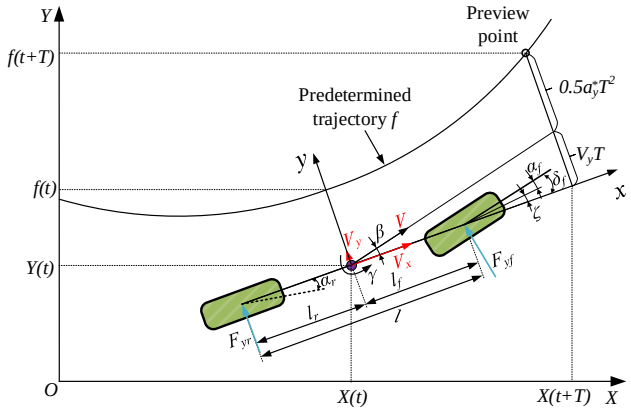

Here, δ_f is the front wheel angle, γ is the yaw rate, a_y^* is the desired lateral acceleration, β is the vehicle sideslip angle, α_f is the sideslip angle of front tyre, α_r is the sideslip angle of rear tyre, l_f is the distance between front axle and centre of vehicle mass, l is the wheelbase, l_r is the distance between rear axle and centre of vehicle mass, F_{yf} is the lateral force of front tyre, F_{yr} is the lateral force of rear tyre, ζ is the heading angle, V_x is the vehicle longitudinal speed,

V is the vehicle speed, V_y is the vehicle lateral speed, T is the preview time.

The preview model assumes that the tracking for the road trajectory can be equivalent to tracking the expected lateral displacement of the vehicle. As shown in Figure 2, the actual lateral displacement of the vehicle is $Y(t)$, and the desired lateral displacement of the vehicle is $f(t)$ at the time t. Assuming that the vehicle is in the constant acceleration state with a desired lateral acceleration, the following equation can be obtained.

$$Y(t+T)=Y(t)+V_yT+\frac{1}{2}a_y^*T^2 \tag{1}$$

Assuming that the actual lateral displacement is as close as possible to the desired lateral displacement after preview time T, the following equation can be obtained based on equation (1).

$$a_y^*=\frac{2}{T^2}\left(f(t+T)-Y(t)-V_yT\right) \tag{2}$$

An expected HW angle δ_{sw}^* can be obtained by the two-degree-of-freedom (2-DOF) vehicle model.

$$\delta_{sw}^*=\frac{a_y^*}{G_{ay}} \tag{3}$$

where G_{ay} is the steady-state gain for the vehicle lateral acceleration on the HW angle.

Based on the equation (2) and equation (3), the expected HW angle is given by

$$\delta_{sw}^*=\frac{1}{G_{ay}}\frac{2}{T^2}\left(f(t+T)-Y(t)-V_yT\right) \tag{4}$$

2.2 Vehicle dynamic model

The 7-DOF vehicle dynamics model is used in this paper, as shown in Figure 3. This is a simplification for the complex nonlinear vehicle model, and its dynamic equations are expressed in equation (5). Only the longitudinal, lateral, and yaw motion of the body and the rotation of the four wheels are analysed (Song, 2016; Ma et al., 2023).

$$\begin{cases} m\left(\dot{V}_x-V_y\gamma\right)=\sum_{i=1}^{4}\left(F_{xi}\cos\delta_i-F_{yi}\sin\delta_i\right) \\ \quad -mgf-C_DA_R\rho_RV_x^2/2 \\ m\left(\dot{V}_y+V_x\gamma\right)=\sum_{i=1}^{4}\left(F_{xi}\sin\delta_i+F_{yi}\cos\delta_i\right) \\ I_z\dot{\gamma}=\sum_{i=1}^{2}\left(F_{xi}\sin\delta_i+F_{yi}\cos\delta_i\right)l_f \\ \quad -\sum_{i=3}^{4}\left(F_{xi}\sin\delta_i+F_{yi}\cos\delta_i\right)l_r \\ +\frac{d}{2}\left(-F_{x1}\cos\delta_1+F_{y1}\sin\delta_1+F_{x2}\cos\delta_2-F_{y2}\sin\delta_2\right. \\ \left.-F_{x3}\cos\delta_3+F_{y3}\sin\delta_3+F_{x4}\cos\delta_4-F_{y4}\sin\delta_4\right) \end{cases} \tag{5}$$

where m is the vehicle mass, F_{xi} is the tyre longitudinal force, F_{yi} is the tyre lateral force, d is the wheel track, C_D is the air resistance coefficient, δ_i is the wheel angle, α_i is the tyre sideslip angle, A_R is the windward area, ρ_R is the air density, I_z is the vehicle moment of inertia around Z-axis, f is the rolling resistance coefficient, g is the gravitational acceleration. Subscripts i = 1, 2, 3 and 4 are the wheels of left front, right front, left rear and right rear respectively. The other symbols are the same as above.

Figure 3 The 7-DOF vehicle dynamic model (see online version for colours)

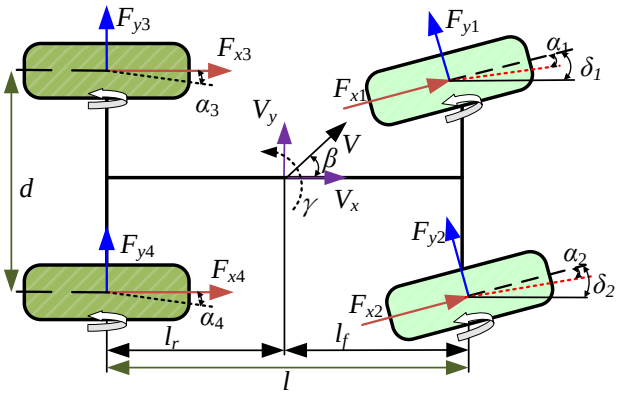

2.3 AFS system dynamic model

Figure 4 shows the dynamic model of the AFS system, and it includes the HW system model, the double-row planetary gear set mechanism model, the AFS motor model, the worm gear-worm mechanism model, and the rack-and-pinion system model. The HW is connected to the sun gear at the upper input end of the double planetary gear sets mechanism through the steering column, and the ring gear of upper row is fixed to the vehicle. The rotation angle of the sun gear of upper row is transmitted to gear mechanism of the lower row through the planetary carrier, and is superimposed with the rotation angle of the ring gear of lower row. Then, it is transmitted to the rack-and-pinion mechanism by the sun gear of lower row. The angle for the ring gear of lower row can be adjusted by the AFS motor and the worm gear-worm mechanism.

Figure 4 AFS system dynamic model

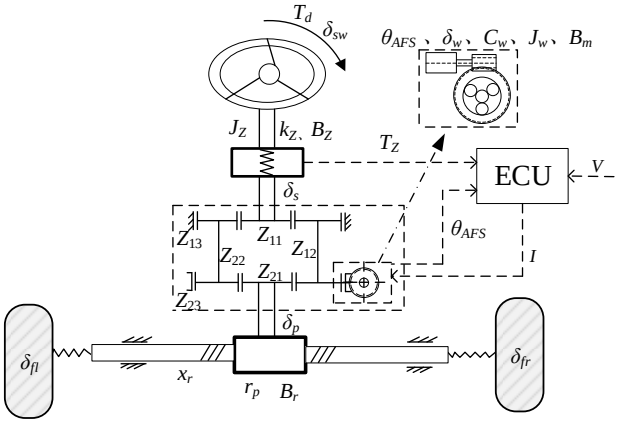

Here, T_d is the HW torque, δ_{sw} is HW angle, J_Z is the moment of inertia of HW and steering column, T_Z is the torque measured on the steering column, δ_s is the input angle of sun gear in double planetary gear sets mechanism, k_Z is the stiffness coefficient of steering column, B_Z is the damping coefficient of steering column, Z_{11} is the teeth number of sun gear in the first stage planetary gear set, Z_{12} is the teeth number of planet gear in the first stage planetary gear set, Z_{13} is the teeth number of outer ring gear in the first stage planetary gear set, Z_{21} is the teeth number of sun gear in the second stage planetary gear set, Z_{22} is the teeth number of planet gear in the second stage planetary gear set, Z_{23} is the teeth number of outer ring gear in the second stage planetary gear set, δ_p is the steering pinion angle, $_{xr}$ is the rack displacement, B_r is the damping coefficient of rack-and-pinion steering gear, δ_w is the output angle of worm gear-worm mechanism, r_p is the radius of steering pinion, θ_{AFS} is the AFS motor angle, I is the current input of AFS motor, J_w is the moment of inertia of worm gear-worm mechanism, B_m is the damping coefficient of AFS motor, C_w is the damping coefficient of worm gear-worm mechanism.

2.3.1 Hand wheel system model

The input of HW system model is the torque T_d, and its output is the input angle δ_s of sun gear in the double planetary gear sets mechanism. The model is constructed with two assumptions. The first is that the mechanical transmission loss between the HW and the steering column is ignored. The second is that the connection between the HW and the steering column is treated as a rigid connection. The dynamic equations for the HW system model are given by

$$J_Z\ddot{\delta}_{sw} + T_Z = T_d - B_Z\dot{\delta}_{sw} \tag{6}$$

$$T_Z + k_Z\delta_s = k_Z\delta_{sw} \tag{7}$$

where the symbols are the same as above.

2.3.2 Double-row planetary gear set model

The double-row planetary gear set mechanism consists of two sets of NGW planetary gear transmission mechanisms. The two sets of NGW planetary gear transmission mechanisms are parallel. It includes two input ends and one output end. One input end is connected to the HW, the other is connected to the AFS motor through a self-locking worm gear-worm mechanism, and the output end is connected to the steering column. The HW angle is superimposed with the output angle of AFS motor to obtain the steering pinion angle δ_p. The transmission characteristic of double planetary gear mechanism is expressed as follows.

$$n_{11} + a_1 n_{13} = (1 + a_1) n_{12} \tag{8}$$

$$n_{21} + a_2 n_{23} = (1 + a_2) n_{22} \tag{9}$$

$$a_1 = Z_{13} / Z_{11},\ a_2 = Z_{23} / Z_{21} \tag{10}$$

where n_{11} is the rotation rate of sun gear at the first stage planetary gear set. n_{12} is the rotation rate of planetary carrier at the first stage planetary gear set. n_{13} is the rotation rate of outer ring gear at the first stage planetary gear set. n_{21} is the rotation rate of sun gear at the second stage planetary gear set. n_{22} is the rotation rate of planetary carrier at the second stage planetary gear set. n_{23} is the rotation rate of outer ring gear at the second stage planetary gear set. a_1 and a_2 are the characteristic parameters of the first and second stage planetary set, respectively. The other symbols are the same as above.

In this paper, a_1 and a_2 in the double-row planetary gear set mechanism are set to be equal, and they are denoted as a. n_{12} is equal to n_{22}, because two sets of NGW planetary gear transmission mechanisms share the same planetary carrier. n_{13} is equal to 0, because the ring gear of upper row is fixed on the vehicle body. Based on the equation (8), equation (9), and the above conditions, the speed relationship between the input and output ends of the AFS system can be expressed as follows.

$$n_{21} = n_{11} \pm a n_{23} \tag{11}$$

The angle relationship between the input and output ends of the AFS system can be expressed as follows.

$$\delta_p = \delta_{sw} \pm \frac{a}{i_w}\theta_{AFS} \tag{12}$$

where i_w is the transmission ratio of worm gear-worm mechanism. The other symbols are the same as above.

2.3.3 AFS motor model

The dynamic model of AFS motor is as follows (Wang et al., 2017).

$$\ddot{\theta}_{AFS} I_m + \dot{\theta}_{AFS} B_m + \dot{\theta}_{AFS} \frac{K_c}{R} K_m = \frac{K_c}{R} U \tag{13}$$

where I_m is the moment of inertia of AFS motor, U is the voltage of AFS motor, R is the armature resistance of AFS motor, K_c is the electromagnetic torque constant of AFS motor, K_m is the electromotive force constant of AFS motor. The other symbols are the same as above.

2.3.4 Worm gear-worm mechanism model

The dynamic model of worm gear-worm mechanism is as follows:

$$J_w\ddot{\delta}_w + C_w\dot{\delta}_w = T_Z + i_w K_m (\theta_{AFS} - i_w\delta_w) \tag{14}$$

where the symbols are the same as above.

2.3.5 Rack-and-pinion system model

The rack-and-pinion system model is adopted as the steering mechanism model in this paper. Its dynamic equation is expressed as follows:

$$m_r\ddot{x}_r + B_r\dot{x}_r + f_r = \frac{K_r}{r_p}\left(\delta_p - \frac{x_r}{r_p}\right) - M_Z \tag{15}$$

where m_r is the equivalent mass of rack, f_r is the friction force of rack-and-pinion steering gear, K_r is the stiffness coefficient of the rack-and-pinion steering gear, M_Z is the steering resistance moment of the rack. The other symbols are the same as above.

3 Ideal VTR control law

3.1 Steady-state yaw rate gain

The 2-DOF model with only lateral motion and yaw motion is employed to obtain steady-state yaw rate gain. The steady-state yaw rate gain is the basis for the analysis of the ideal VTR of the AFS system. Figure 5 displays the 2-DOF model.

Figure 5 2-DOF model (see online version for colours)

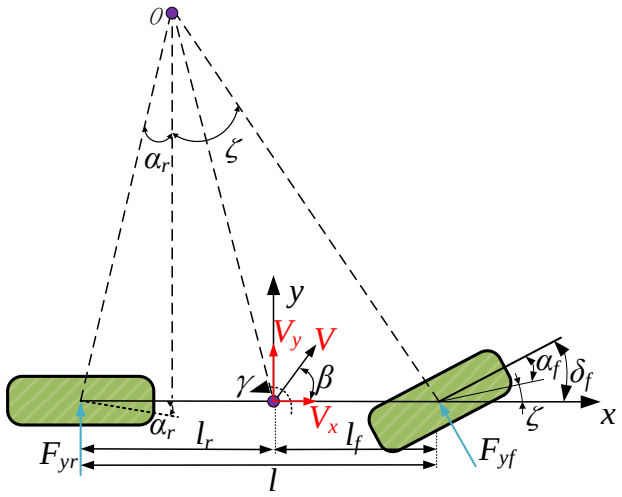

The differential equation for 2-DOF vehicle dynamic reference model is given by (Ti et al., 2022):

$$\begin{cases} (k_1 + k_2)\beta + \dfrac{1}{V_x}(l_f k_1 - l_r k_2)\gamma - k_1\delta_f = m(\dot{V}_y + V_x\gamma) \\ (l_f k_1 - l_r k_2)\beta + \dfrac{1}{V_x}(l_f{}^2 k_1 + l_r{}^2 k_2)\gamma - l_f k_1\delta_f = I_Z\dot{\gamma} \end{cases} \tag{16}$$

where k_1 is the cornering stiffness of front wheel, δ_f is front wheel angle, k_2 is the cornering stiffness of rear wheel. The other symbols are the same as above.

When the vehicle reaches steady-state in step input condition, $\dot{V}_y = 0$, $\dot{\gamma} = 0$. Based on equation (16) and $\dot{V}_y = 0$, $\dot{\gamma} = 0$, the steady-state yaw rate gain can be expressed as follows:

$$\begin{cases} G_{fw} = \dfrac{\gamma}{\delta_f} = \dfrac{V_x / l}{1 + KV_x{}^2} \\ K = m\left(l_f / k_2 - l_r / k_1\right)/l^2 \end{cases} \tag{17}$$

where G_{fw} is the steady-state yaw rate gain, K is the stability factor. The other symbols are the same as above.

3.2 Steering transmission ratio characteristics with vehicle speed

The steering transmission ratio has a significant impact on the vehicle handling performance. In order to reduce the driving burden and improve vehicle safety, the vehicle needs to have better steering sensitivity at the low-speed segment and better steering stability at the high-speed segment. The above requirements can be met by the VTR law, which is based on the principle of constant gain for steady-state vehicle system.

The constant gain for steady-state vehicle system can be expressed as follows (Wu and Li, 2020).

$$G_w = \frac{\gamma}{\delta_{sw}} \tag{18}$$

where G_w is the constant gain for steady-state vehicle system. The other symbols are the same as above.

Combining equations (17) and (18), the VTR i can be expressed as follows.

$$i = \frac{\delta_{sw}}{\delta_f} = \frac{V_x / l}{1 + KV_x{}^2} \cdot \frac{1}{G_w} \tag{19}$$

The VTR calculated by equation (19) has the problem of being too small at the low-speed segment and too large at the high-speed segment. If the transmission ratio is too small at the low-speed segment, it is difficult to meet the need for steering sensitivity. If the transmission ratio is too large at the high-speed segment, it is difficult to meet the need for steering stability. For that, the law of ideal VTR dependent on vehicle speed is studied based on the segmented design of vehicle speed. The vehicle speed is divided into low-speed, medium-speed and high-speed segments in this paper. Among them, 0–30 km/h is defined as the low-speed segment, 30–90 km/h is defined as the medium-speed segment, and greater than 90 km/h is defined as the high-speed segment.

The transmission ratio is set to $i_{\min}$ at the low-speed segment. Where $i_{\min}$ is the minimum value of the transmission ratio at the medium-speed segment, that is, $i_{\min} = f(30)$. The transmission ratio is set to $i_{\max}$ at the high-speed segment. Where, $i_{\max}$ is the maximum value of the transmission ratio at the medium-speed segment, that is, $i_{\max} = f(90)$.

The original VTR law at the full vehicle speed range can be expressed as follows.

$$i = \begin{cases} i_{\min} & (0 \le V_x \le 30) \\ \dfrac{V_x / l}{1 + KV_x{}^2} \cdot \dfrac{1}{G_w} & (30 < V_x < 90) \\ i_{\max} & (90 \le V_x) \end{cases} \tag{20}$$

where $i_{\min} = f(30) = 30 / (l * (1 + K*30*30)*G_w)$, $i_{\max} = f(90) = 90 / (l * (1 + K*90*90)*G_w)$.

The rotation angle of AFS motor can be calculated by equation (21). The angular acceleration of AFS motor will fluctuate greatly, when the vehicle accelerates or decelerates at the critical speed. This will lead to mechanical vibration and energy loss, and will affect the performance of AFS motor.

$$\theta_{AFS}=\begin{cases}\delta_{sw}\left(\dfrac{i_p}{i_{\min}}-1\right)\dfrac{i_w}{a} & 0\le V_x\le 30\\ \delta_{sw}\left(\dfrac{i_p}{V_x/l}\left(G_w\times\left(1+KV_x^2\right)\right)-1\right)\dfrac{i_w}{a} & 30\le V_x\le 90\\ \delta_{sw}\left(\dfrac{i_p}{i_{\max}}-1\right)\dfrac{i_w}{a} & V_x>90\end{cases} \quad (21)$$

For solving the problem above, the improved S-type function is employed to fit and optimise the equation (20). The formula for the improved S-type function is expressed as follows.

$$i_{IS}=f_s\left(V_x\right)=\frac{\left(i_{\max}-i_{\min}\right)}{\left(1+e^{-\varepsilon\left(V_x-\tau\right)}\right)}+i_{\min} \quad (22)$$

where ε and τ are the adjustment coefficients for the VTR curve.

As shown in equation (22), the proximity between the fitted curve and the original curve is determined by the curve adjustment coefficients, so the PSO algorithm is employed to optimise them. The PSO algorithm is started with a certain number of randomly generated particles, and finds the optimal solution through iterations. It evaluates the solution quality by fitness, and can get the optimal solution quickly. Figure 6 shows the optimisation process.

The particle swarm size is set to 100, the dimension is set to 2, the maximum number of iterations is set to 100, and the maximum speed of particle movement is taken as 15% of the variation range for each dimensional variable of the particle. In each iterative optimisation, the velocity and position of the particles can be dynamically adjusted according to the local optimal value and the global optimal value. The update equations for the velocity and position are expressed as follows (Khajeh and Ghasemi, 2019; Zhao et al., 2021).

$$\begin{cases}v_{i,j}(t+1)=w_b v_{i,j}(t)+c_1 r_1\left[p_{i,j}(t)-x_{i,j}(t)\right]+c_2 r_2\left[p_{g,j}(t)-x_{i,j}(t)\right]\\ x_{i,j}(t+1)=x_{i,j}(t)+x_{i,j}(t+1)\qquad i=1,2,\cdots,I\qquad j=1,2,\cdots,J\end{cases} \quad (23)$$

where notation i is the swarm size and j is the search space dimension. x_i, $j(t+1)$ is defined as the position of j^{th} dimension of i^{th} particle at $t+1^{\text{th}}$ iteration. v_i, $j(t+1)$ is defined as the velocity of j^{th} dimension of i^{th} particle at $t+1^{\text{th}}$ iteration. $p_{i,j}(t)$ is the best position. $p_{g,j}(t)$ is the best position. w_b is inertia weight. r_1 and r_2 are the random numbers between 0 and 1. c_1 cognitive parameter, and c_2 are is the social scaling parameter.

In the control process of AFS, the difference between the VTR curve optimised by the improved S-type function and the original VTR curve should be minimised as much as possible. This can reduce the driver's driving burden and improve the vehicle safety. For that, the sum of squared errors between the original VTR curve and the VTR curve optimised by improved S-type function is taken as the optimisation objective.

Figure 6 The flowchart for the optimisation of curve adjustment coefficients

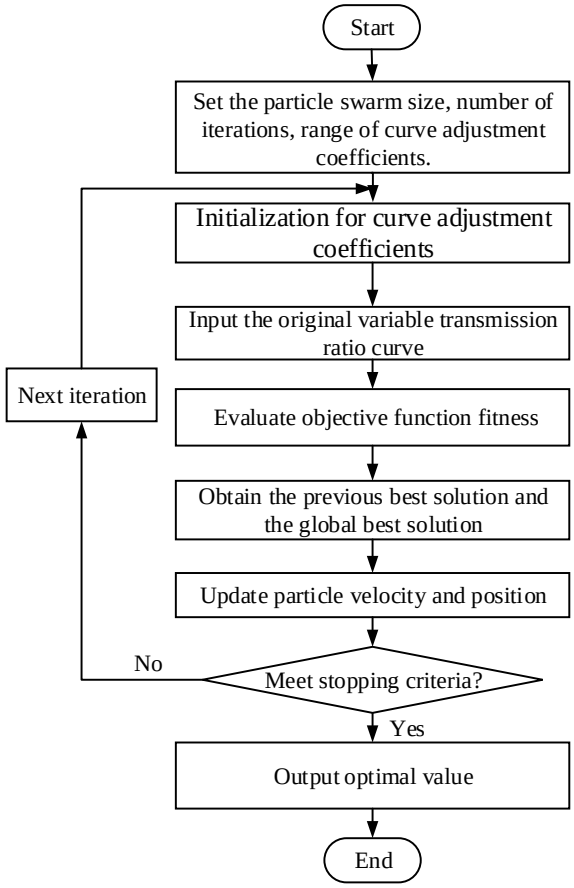

The optimisation objective is expressed as follow.

$$Y\left(V_x\right)=\int\left(i-i_{IS}\right)^2 dV_x \quad (24)$$

The symbols are the same as above.

According to equation (22), the shape of the optimised curve is determined by the curve adjustment coefficient ε and τ. For that, the curve adjustment coefficients are utilised as the optimisation variables. By preliminary testing, the optimised curve is closer to the original VTR curve when the interval of ε is set as [0, 1] and the interval of τ is set as [20, 80]. For that, the above range of values is set as the constraints for ε and τ.

The optimisation objectives, optimisation variables and constraints are as follow.

$$\begin{cases}\min Y\left(V_x\right)=\int\left(i-i_{IS}\right)^2 dV_x\\ \text{where}\quad y_{PSO}=[\varepsilon,\tau]^T\\ s.t.\quad 0<\varepsilon<1,\ 20<\tau<80\end{cases} \quad (25)$$

The iterative process for the fitness function value is shown in Figure 7. The iterative process for the curve adjustment coefficients is shown in Figure 8.

Figure 7 The fitness function

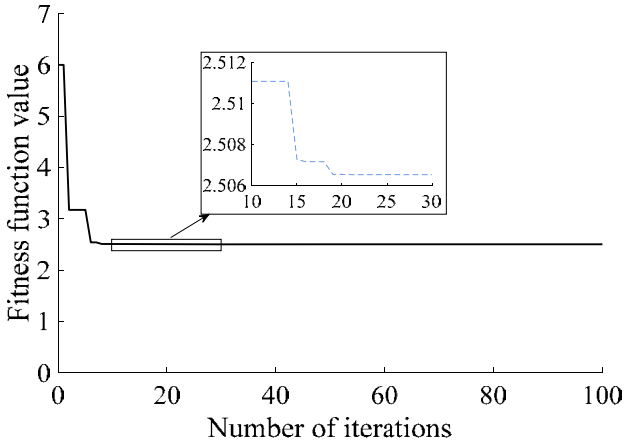

Figure 8 The curve adjustment coefficients (see online version for colours)

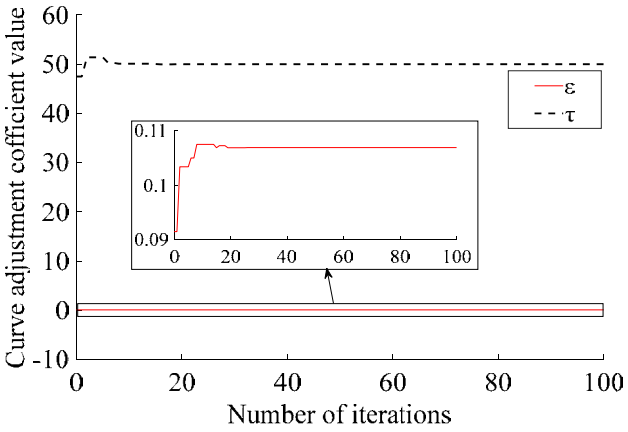

Based on the Figure 7 and 8, the fitness function value reaches the minimum value after 19th iterations. The optimal values of the curve adjustment coefficients are 0.1069 and 49.9837, respectively.

The original curve and optimised curve are shown in Figure 9, and the original curve is obtained based on equation (20). Taking the HW input of 45° as an example, the comparison for AFS motor angular acceleration before and after optimisation is shown in Figure 10.

As shown in Figure 9, the optimised curve can track the original curve at the medium speed segment, and the optimised curve transition is smoother at the critical speed. This can avoid the sudden change of angular acceleration caused by the original curve effectively. As shown in Figure 10, the angular acceleration of the AFS motor will undergo a significant sudden change at the critical speed when the original VTR curve is used. When using the optimised VTR curve, the angular acceleration variation of the AFS motor is relatively smooth throughout the entire vehicle speed range. This proves the effectiveness of the improved S-type function in optimising the VTR curve.

Figure 9 The VTR curve (see online version for colours)

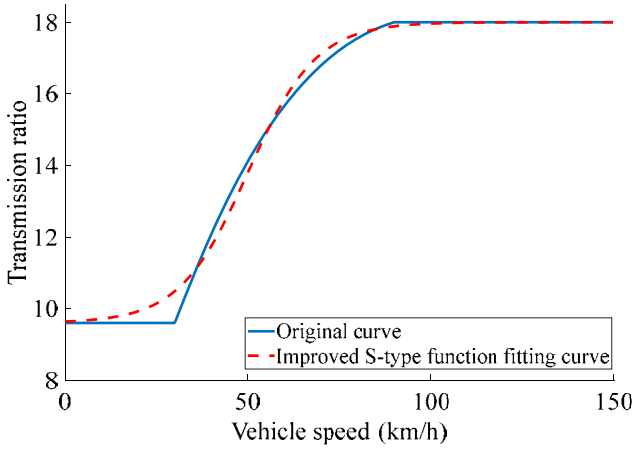

Figure 10 The angular acceleration of AFS motor (see online version for colours)

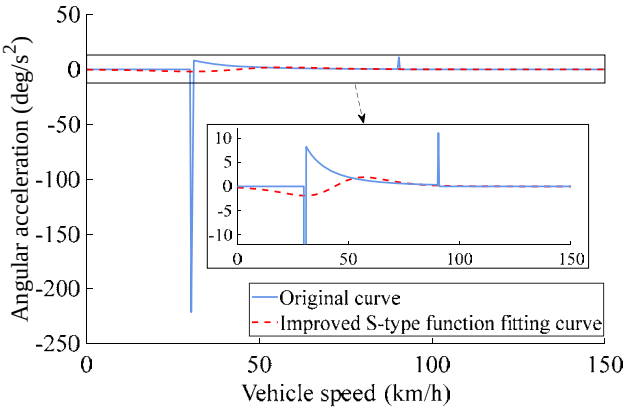

3.3 Steering transmission ratio characteristics with vehicle speed and hand wheel angle

When the HW angle is in the middle position, the vehicle is expected to keep in a straight line. But the straight-line driving state may be affected by the uncertain operation of the driver. Therefore, a larger transmission ratio is used to reduce the negative impact of uncertain swinging of the HW at the centre position. When the HW moves away from the centre position, it indicates that steering behaviour has occurred. For that, a smaller transmission ratio is used to improve the sensitivity of steering operations. They are implemented by the cosine function in this paper. The reason for that is the cosine function is symmetric about the y-axis and has the maximum value at zero. For adjusting the influence of the HW on the VTR, an influencing factor is added to the formula.

Based on equation (20), equation (22), the results of PSO and the above analysis, the ideal VTR with vehicle speed and HW angle can be expressed as follows.

$$i = \frac{8.4}{1+e^{-0.1069(V_x-49.9837)}} + 9.6 + G_{sw}\cos\left(\frac{\delta_{sw}}{2}\right) \tag{26}$$

where G_{sw} is the influence factor for HW angle. The other symbols are the same as above.

Figure 11 The optimised VTR surface (see online version for colours)

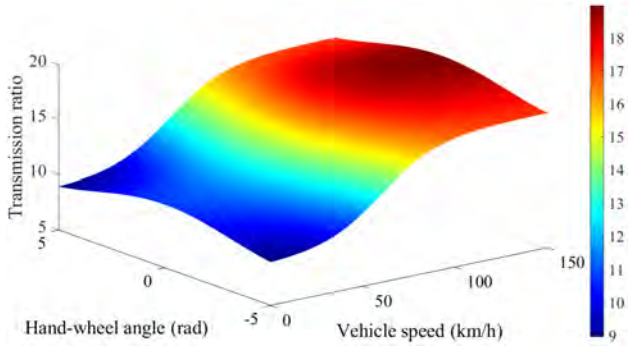

Based on equation (26), the optimised VTR surface is shown in Figure 11. Figure 11 displays the transmission ratio is small at the low-speed segment, and this can meet the need for steering sensitivity. The transmission ratio will increase rapidly and steadily at the medium-speed segment. The transmission ratio becomes larger and tends to be stable at the high-speed segment, and this can meet the need for steering stability. When the vehicle speed is the same, the transmission ratio will vary with the HW angle. The transmission ratio is larger when the HW angle is in the middle position area. The transmission ratio becomes smaller along with the increase of the HW angle.

4 Control system design

Figure 12 displays the overall structure for AFS control system. The VTR model calculates the process angle δ_{vt} based on vehicle speed v and HW angle δ_{sw}. The desired yaw rate γ_d and desired vehicle sideslip angle β_d are obtained by the 2-DOF model. The input variables of the 2-DOF model are the process angle δ_{vt} and vehicle speed v. Actual yaw rate γ and actual vehicle sideslip angle β are used as feedback variables of the control system. Actual yaw rate γ and actual vehicle sideslip angle β are obtained by the 7-DOF model. Three sets of control variables are adopted by the LQR controller to determine the additional steering angle $\Delta\delta_{vt}$. Three sets of control variables are the process angle δ_{vt}, desired yaw rate γ_d and desired vehicle sideslip angle β_d, and the error between actual value and desired value. The additional steering angle $\Delta\delta_{vt}$ is superimposed with the process angle δ_{vt} to obtain the desired front wheel angle δ_{df}. The desired AFS motor angle δ_{dAFS} is obtained by the AFS angle calculation module, and it is used in the AFS motor model. The actual AFS motor angle δ_{aAFS} is superimposed with the HW angle δ_{sw}, and the actual front wheel angle δ_{af} is obtained by the rack-and-pinion system model. The actual front wheel angle δ_{af} is adopted by the 7-DOF vehicle dynamics model to implement the closed-loop control.

Figure 12 Overall structure of AFS system (see online version for colours)

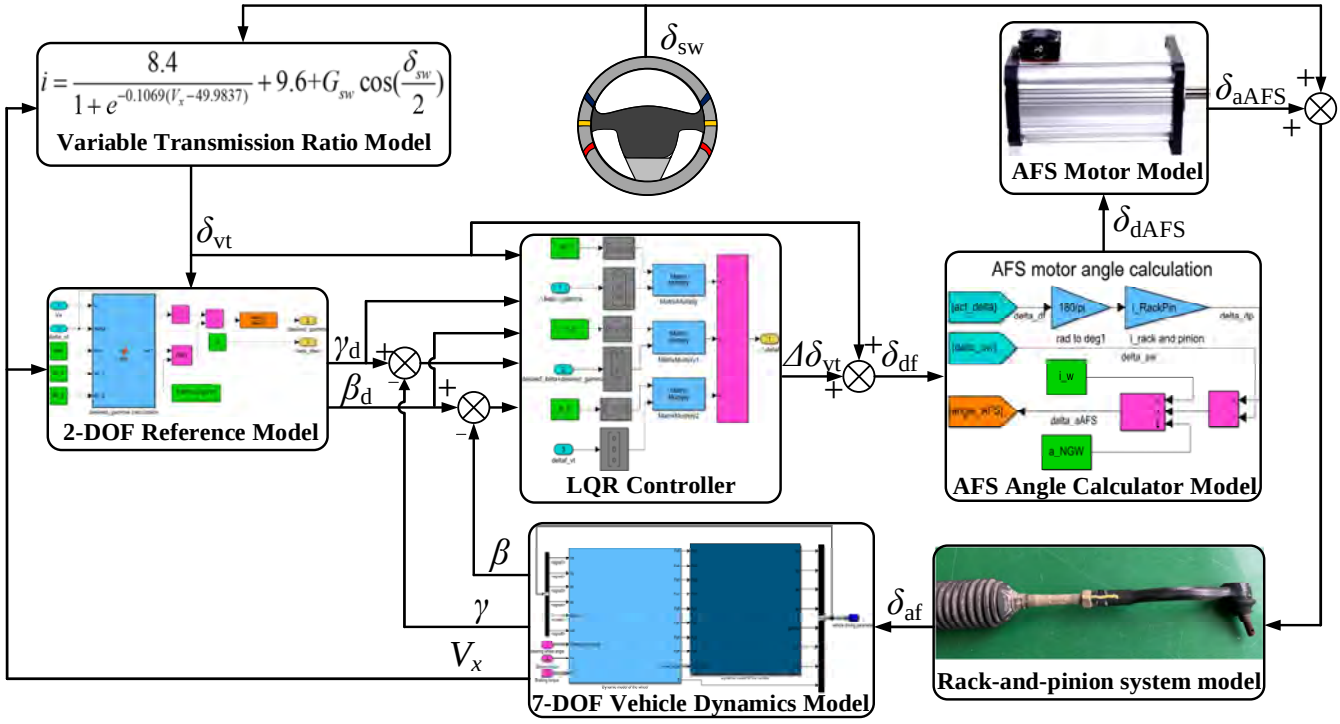

Here, δ_{vt} is the process angle of VTR model, $\Delta\delta_{vt}$ is the additional steering angle, δ_{df} is the desired front wheel angle, δ_{dAFS} is the desired AFS motor angle, δ_{aAFS} is the actual AFS motor angle, δ_{af} is the actual front wheel angle, γ_d is the desired yaw rate, β_d is the desired vehicle sideslip angle. The other symbols are the same as above.

4.1 Desired value calculation

Based on equation (16), the yaw rate when vehicle reaches steady state can be obtained by

$$\gamma = \frac{V_x / l}{1 + KV_x{}^2}\delta_{vt} \tag{27}$$

The desired yaw rate is also constrained by the road adhesion coefficient, and the corresponding expression is as follows.

$$\gamma_{\max} \le \frac{\mu g}{V_x} \tag{28}$$

The desired yaw rate can be obtained by:

$$\begin{cases} \gamma_d = \min\left(\dfrac{V_x / l}{1 + KV_x{}^2}\cdot|\delta_{vt}|, \dfrac{\mu g}{V_x}\right)\operatorname{sgn}(\delta_{vt}) \\ \operatorname{sgn}(x) = \begin{cases} 1, & x > 0 \\ 0, & x = 0 \\ -1, & x < 0 \end{cases} \end{cases} \tag{29}$$

where μ is the road adhesion coefficient. The other symbols are the same as above.

For making the transition of the vehicle yaw rate smoother and avoiding excessive fluctuations during control, a first-order inertia element is employed to correct it. The corrected desired yaw rate γ_d is expressed as follows.

$$\gamma_d = \min\left(\frac{V_x / l}{1 + KV_x{}^2}\cdot|\delta_{vt}|, \frac{\mu g}{V_x}\right)\operatorname{sgn}(\delta_{vt})\cdot\frac{1}{1+\tau_w s} \tag{30}$$

where τ_w is the constant of response time. The other symbols are the same as above.

In order to maintain a good body posture during the steering process, the vehicle sideslip angle should be as small as possible. The desired sideslip angle β_d can be obtained by:

$$\beta_d = 0 \tag{31}$$

Equation (30) and equation (31) can be expressed as the space equation.

$$\begin{cases} X_d = \begin{bmatrix} \beta_d \\ \gamma_d \end{bmatrix} \\ Y_d = CX_d \end{cases} \tag{32}$$

where $C = \begin{bmatrix} 1 & 0 \\ 0 & 1 \end{bmatrix}$.

4.2 LQR controller design

The equation (16) is augmented in a state-space form.

$$\begin{cases} \dot{X} = AX + B\delta_{vt} + B\Delta\delta_{vt} \\ Y = DX \end{cases} \tag{33}$$

where

$$X = \begin{bmatrix} \gamma \\ \beta \end{bmatrix}, A = \begin{bmatrix} \dfrac{k_f + k_r}{mV_x} & \dfrac{l_f k_f - l_r k_r}{mV_x^2} - 1 \\ \dfrac{l_f k_f - l_r k_r}{I_Z} & \dfrac{l_f^2 k_f + l_f^2 k_r}{I_Z V_x} \end{bmatrix}, B = \begin{bmatrix} -\dfrac{k_f}{mV_x} \\ -\dfrac{l_f k_f}{I_Z} \end{bmatrix}, D = \begin{bmatrix} 1 & 0 \\ 0 & 1 \end{bmatrix}.$$

The other symbols are the same as above.

The design goal of LQR controller is used to discover the optimal control law for additional steering angle. It can make the response parameters of 7-DOF model to track the desired value from 2-DOF model, and minimise the state tracking errors. The state tracking error e is expressed as follows.

$$e = Y - Y_d \tag{34}$$

For seeking optimal control law for additional steering angle, the performance index J should reach minimum. The expression of J can be obtained by:

$$J = \frac{1}{2}\int_{t_0}^{t_f}\left[(Y - Y_d)^T Q(Y - Y_d) + \Delta\delta_{vt}{}^T R\Delta\delta_{vt}\right]dt \tag{35}$$

Combining equations (32) to (35), the performance index J can be obtained by

$$J = \frac{1}{2}\int_{t_0}^{t_f}\left[(X - X_d)^T Q(X - X_d) + \Delta\delta_{vt}{}^T R\Delta\delta_{vt}\right]dt \tag{36}$$

Q and R are the weight coefficient matrices and they are expressed as follows.

$$Q = \begin{bmatrix} w_1 & 0 \\ 0 & w_2 \end{bmatrix} \quad R = [w_3] \tag{37}$$

where w_1, w_2, and w_3 are the weight coefficients of LQR controller, and they indicate the importance degree of the LQR controller on different vehicle parameters. w_1 indicates the importance degree on sideslip angle, and w_2 indicates the importance degree on yaw rate. w_3 indicates the importance degree on the control variable.

For obtaining J, the Hamiltonian function is constructed based on the maximum principle, and it is expressed as:

$$\begin{aligned} H = {} & \frac{1}{2}(X - X_d)^T Q(X - X_d) + \frac{1}{2}\Delta\delta_{vt}{}^T R\Delta\delta_{vt} \\ & + \lambda\left[AX + B\delta_{vt} + B\Delta\delta_{vt}\right] \end{aligned} \tag{38}$$

The optimal control law for additional steering angle $\Delta\delta_{vt}$ can be expressed as:

$$\Delta\delta_{vt} = -R^{-1}B^T\lambda \tag{39}$$

The accompanying equation is expressed as follows.

$$\dot{\lambda} = -\frac{\partial H}{\partial X} = -Q(X - X_d) - A^T \lambda \tag{40}$$

Assuming $\lambda = PX - \varepsilon$, its derivative can be expressed as follows.

$$\dot{\lambda} = \dot{P}X + P\dot{X} - \dot{\varepsilon} \tag{41}$$

where P and ε are the intermediate calculated variables.

When the system reaches steady state, $\dot{P} = \dot{\varepsilon} = 0$, and equation (41) is converted to the following equation.

$$\dot{\lambda} = P\dot{X} \tag{42}$$

Combining equations (33), (39) and (42) arrives at the following equation.

$$\dot{\lambda} = PAX - PBR^{-1}B^T PX + PBR^{-1}B^T \varepsilon + PB\delta_{vt} \tag{43}$$

Combining equations (40) and (43) arrives at the following equation.

$$\begin{aligned}\left(PA + A^T P - PBR^{-1}B^T P + Q\right) X = (A^T - PBR^{-1}B^T)\varepsilon \\ + QX_d - PB\delta_{vt}\end{aligned} \tag{44}$$

Based on the arbitrariness of X, the Riccati algebraic equations are obtained.

$$\begin{cases} PA + A^T P - PBR^{-1}B^T P + Q = 0 \\ (A^T - PBR^{-1}B^T)\varepsilon + Qx_d - PB\delta_{vt} = 0 \end{cases} \tag{45}$$

The expressions for P and ε can be obtained from equation (45), and they are substituted into equation (39) to get the optimal control law as follows.

$$\begin{aligned}\Delta\delta_{vt} = -R^{-1}B^T PX - R^{-1}B^T (A^T - PBR^{-1}B^T)^{-1} QX_d \\ + R^{-1}B^T (A^T - PBR^{-1}B^T)^{-1} PB\delta_{vt}\end{aligned} \tag{46}$$

The best additional steering angle $\Delta\delta_{vt}$ can be obtained as follows.

$$\Delta\delta_{vt} = -K_1 e - K_2 X_d + K_3 \delta_{vt} \tag{47}$$

where $K_1 = R^{-1}B^T P$, $K_2 = R^{-1}B^T(A^T + P - PBR^{-1}B^T)^{-1}Q$, $K_3 = R^{-1}B^T(A^T - PBR^{-1}B^T)^{-1}PB$. The other symbols are the same as above.

5 Results and verification

The effectiveness of the comprehensive control based on VTR theory and LQR algorithm is verified, the comparisons between fixed transmission ratio and VTR control under four conditions are analysed. Four conditions are HW angle step input at low-speed, HW angle step input at medium-speed, HW sine input at high-speed, and double lane change (DLC) at high-speed.

5.1 Condition 1: hand-wheel angle step input at low-speed

To analysis the effectiveness of the comprehensive control, the HW angle δ_{sw} is set as a step angle input, with an input angle of 1.74 rad in the Figure 13. The vehicle runs at a constant longitudinal speed v = 20 km/h on a high friction-coefficient road with μ = 0.85.

The responses of steering transmission ratio are shown in Figure 14. Figure 15 shows the responses of yaw rate and vehicle sideslip angle. The maximum values of e_γ and e_β at peak under fixed transmission ratio, VTR control, and comprehensive control are shown in Table 1. Table 2 displays the maximum values of e_γ and e_β at stable. The angle responses of each steering mechanism are shown in Figure 16 and Table 3.

Figure 13 Hand-wheel angle (v = 20 km/h and μ = 0.85)

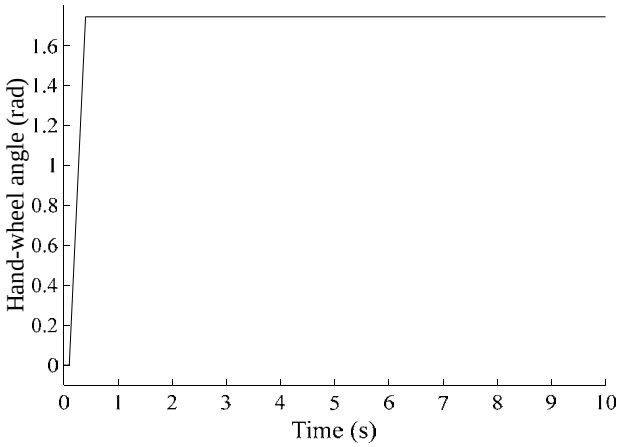

Figure 14 Transmission ratio response (v = 20 km/h, μ = 0.85 and δ_{sw} = 1.74 rad)

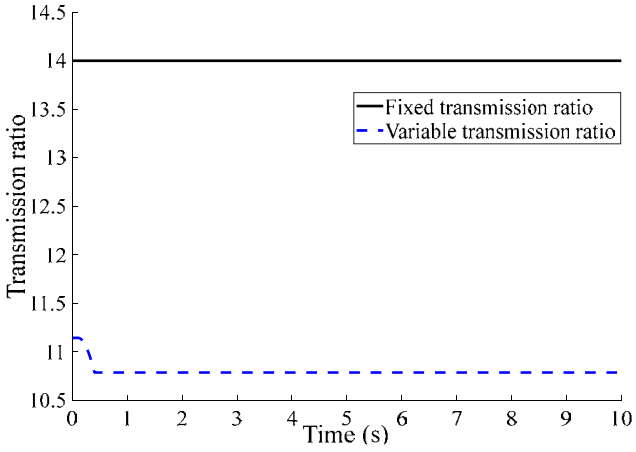

In order to better improve manoeuvrability at low speeds, the transmission ratio under VTR control is smaller than that of fixed transmission ratio, as shown in Figure 14. This proves that VTR control can meet the sensitivity requirements for low-speed steering. When the HW is at the middle position, the transmission ratio is large, and this is conducive to cutting down the error of steering wheel input. As shown in Figure 15, Table 1, and Table 2, the vehicle yaw rate for VTR control and comprehensive control can well track the desired values under HW step input at low-speed condition, and the control error of comprehensive control is the smallest. Correspondingly, the vehicle sideslip angles under VTR control and comprehensive control are

greater. The reason for that is the steering wheel angle under VTR control is larger than the fixed transmission ratio for greater manoeuvrability.

Figure 15 (a) Yaw rate responses (b) Vehicle sideslip angle responses (see online version for colours)

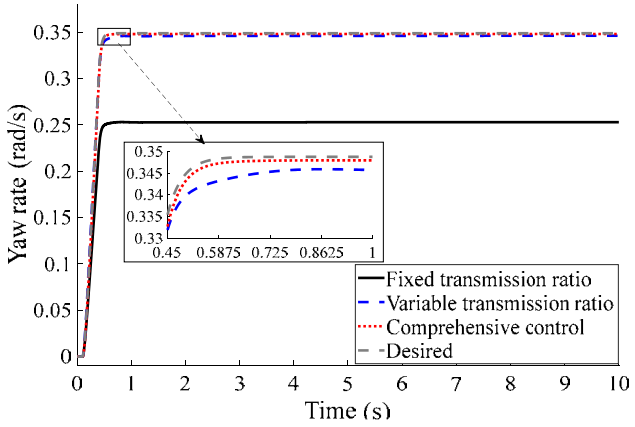

(a)

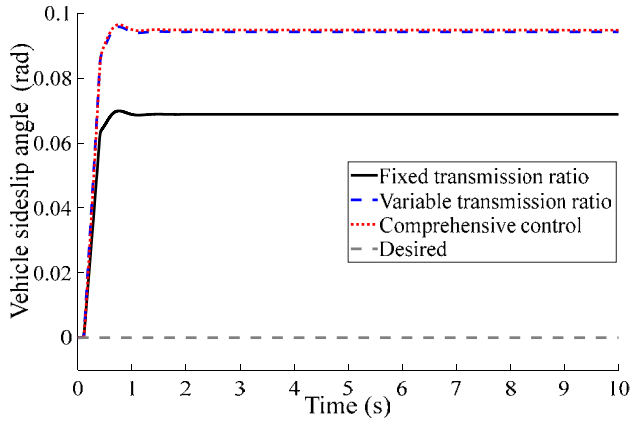

(b)

Table 1 The maximum values of e_γ and e_β at peak

Control scheme	e_γ *(rad/s)*	e_β *(rad)*
Fixed transmission ratio	0.0968	0.0699
Variable transmission ratio control	0.0065	0.0958
Comprehensive control	0.0054	0.0965

Table 2 The maximum values of e_γ and e_β at stable

Control scheme	e_γ *(rad/s)*	e_β *(rad)*
Fixed transmission ratio	0.0960	0.0688
Variable transmission ratio control	0.0028	0.0943
Comprehensive control	0.0008	0.0949

Based on Figure 16 and Table 3, the rotation direction for the HW and AFS motor are the same under VTR control and comprehensive control. This can increase the front wheel angle to improve steering sensitivity at low speed.

Figure 16 The angle responses of each steering mechanism (v = 20 km/h, μ = 0.85 and δ_{sw} = 1.74 rad) (see online version for colours)

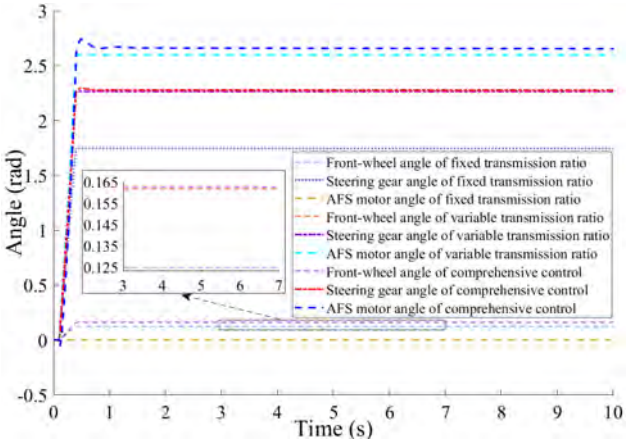

Table 3 The angle of mechanisms at stable

Control scheme	*Front wheel (rad)*	*Steering gear (rad)*	*AFS motor (rad)*
Fixed transmission ratio	0.1247	1.740	0
Variable transmission ratio control	0.1628	2.265	2.598
Comprehensive control	0.1626	2.277	2.659

5.2 Condition 2: hand-wheel angle step input at medium-speed

The HW angle is set as a step angle input, with an input angle of 0.35 rad in Figure 17. The operating conditions are a high friction coefficient road with 0.85 and a constant speed of 80 km/h. Figure 18 shows the response of steering transmission ratio. Figure 19 displays the responses of yaw rate and sideslip angle. The maximum values of e_γ and e_β at peak under fixed transmission ratio, VTR control, and comprehensive control are shown in Table 4. The maximum values of e_γ and e_β at stable are shown in Table 5.

Figure 17 Hand-wheel angle (v = 80 km/h and μ = 0.85)

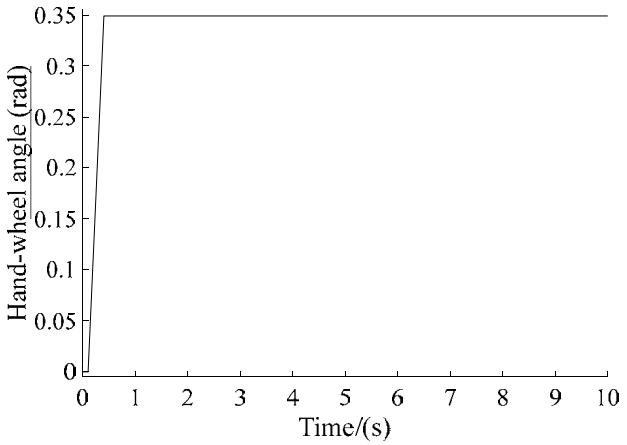

Figure 18 Transmission ratio response (v = 80 km/h, μ = 0.85 and δ_{sw} = 0.35 rad) (see online version for colours)

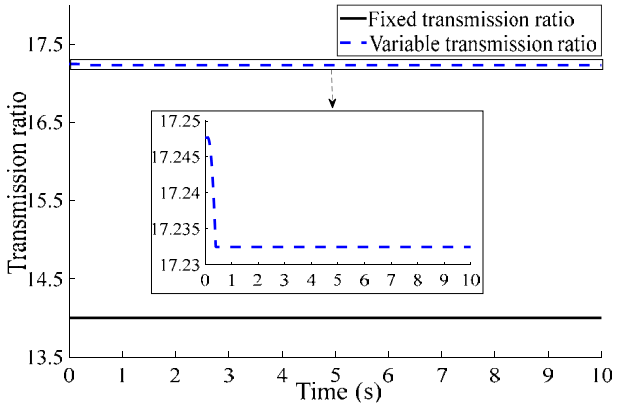

Figure 19 (a) Yaw rate responses (b) Vehicle sideslip angle responses (v = 80 km/h, μ = 0.85 and δ_{sw} = 0.35 rad) (see online version for colours)

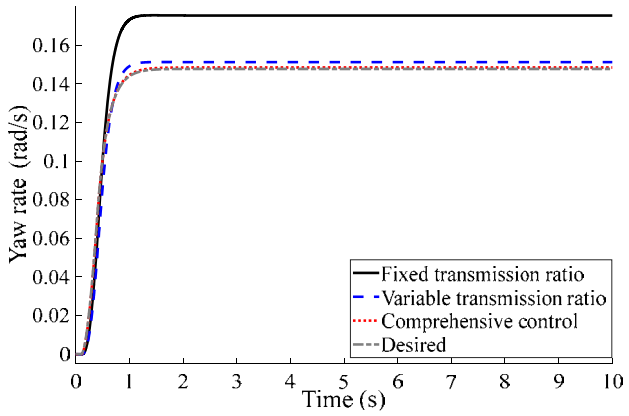

(a)

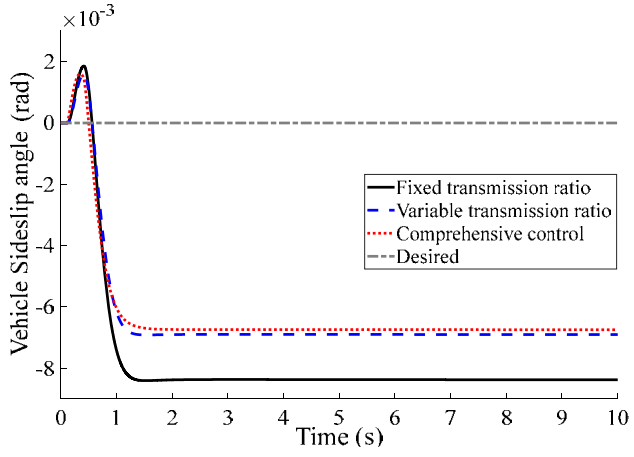

(b)

Table 4 The maximum values of e_γ and e_β at peak

Control scheme	e_γ *(rad/s)*	e_β *(rad)*
Fixed transmission ratio	0.0293	0.0085
Variable transmission ratio control	0.0209	0.0070
Comprehensive control	0.0015	0.0067

Table 5 The maximum values of e_γ and e_β at stable

Control scheme	e_γ *(rad/s)*	e_β *(rad)*
Fixed transmission ratio	0.0277	0.0084
Variable transmission ratio control	0.0035	0.0069
Comprehensive control	0.0008	0.0067

Figure 18 shows that the steering transmission ratio under VTR control is greater than that of fixed transmission ratio when the vehicle is running at medium-speed. At this time, the vehicle stability is more important. Based on Figure 19, Table 4 and Table 5, the peak and stable values of the vehicle response parameters under VTR control and comprehensive control can be decreased, and the vehicle response parameters under comprehensive control are closer to desired values. According to Table 5, the maximum errors e_γ under fixed transmission ratio, VTR control, and comprehensive control are 18.71%, 2.37%, and 0.5%, respectively. The vehicle sideslip angle under VTR control and comprehensive control is smaller than fixed transmission ratio obviously, and is closer to desired value. Compared with fixed transmission ratio scheme, the errors e_γ and e_β under VTR and comprehensive control are smaller with a small HW angle at medium speed. Both control methods have good effect on improving the vehicle stability, and the effect of comprehensive control is better.

The vehicle response under large HW angle step input at medium speed is also necessary, because the risk for vehicle destabilisation will increase sharply. The HW angle is set to an angular step input 1.74 rad, as shown in Figure 13. The vehicle runs at a constant longitudinal speed v = 80 km/h on a high friction-coefficient road with μ = 0.85. Figure 20 displays the response of the transmission ratio. Figure 21 shows the responses of vehicle sideslip angle and yaw rate. The maximum value of e_γ and e_β at peak under fixed transmission ratio, VTR control, and comprehensive control is shown in Table 6. The maximum values for e_γ and e_β at stable are shown in Table 7. The angle responses of each steering mechanism are shown in Figure 22 and Table 8.

Figure 20 Transmission ratio response (v = 80 km/h, μ = 0.85 and δ_{sw} = 1.74 rad) (see online version for colours)

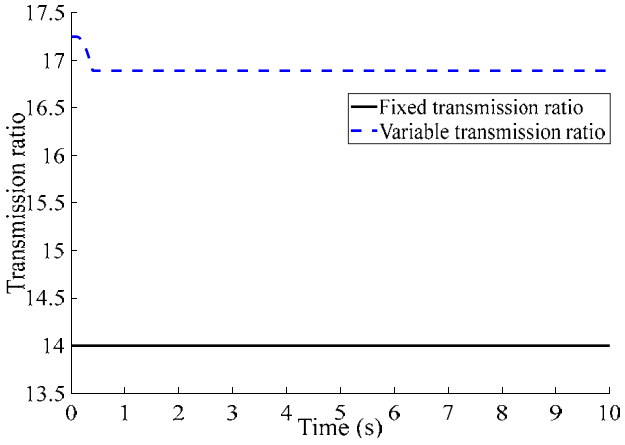

Figure 21 (a) yaw rate responses (b) vehicle sideslip angle responses (v = 80 km/h, μ = 0.85 and δ_{sw} = 1.74 rad) (see online version for colours)

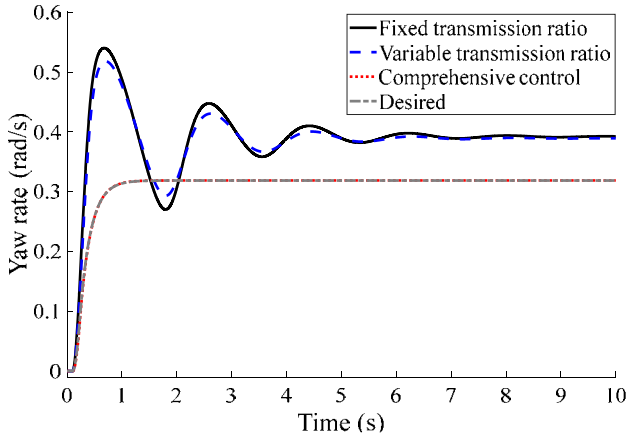

(a)

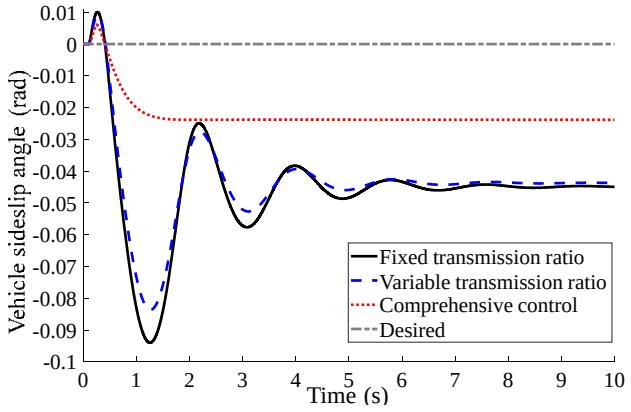

(b)

Table 6 The maximum values of e_γ and e_β at peak

Control scheme	e_γ *(rad/s)*	e_β *(rad)*
Fixed transmission ratio	0.2538	0.0940
Variable transmission ratio control	0.2281	0.0836
Comprehensive control	0.0056	0.0238

Table 7 The maximum values of e_γ and e_β at stable

Control scheme	e_γ *(rad/s)*	e_β *(rad)*
Fixed transmission ratio	0.0724	0.0499
Variable transmission ratio control	0.0701	0.0437
Comprehensive control	0.0001	0.0238

Figure 20 shows that the steering transmission ratio under VTR control is greater than that of fixed transmission ratio. When the HW is in the middle position, the transmission ratio is large, and this is conducive to reduce the error of HW input. It is conducive to improve the stability of straight driving. Based on Figure 21, Table 6 and Table 7, the response parameters of vehicle state can reach stable values faster under comprehensive control, and the transition for comprehensive control is smoother. The vehicle response parameters under comprehensive control are closer to desired values. The maximum values of e_γ are 27.73%, 22%, and 0.1% under fixed transmission ratio, VTR control, and comprehensive control, respectively. The vehicle sideslip angle under comprehensive control is closer to desired value, and it is much smaller than the value of the VTR control. The vibration amplitude for vehicle response parameters is large when the HW angle is set to a large angular step input at medium speed under VTR control. This may lead to lose of stability during the steering process. The comprehensive control still has a good control effect, and it can significantly improve the vehicle driving stability with large step input at medium-speed.

Figure 22 The angle responses of each steering mechanism (v = 80 km/h, μ = 0.85 and δ_{sw} = 1.74 rad) (see online version for colours)

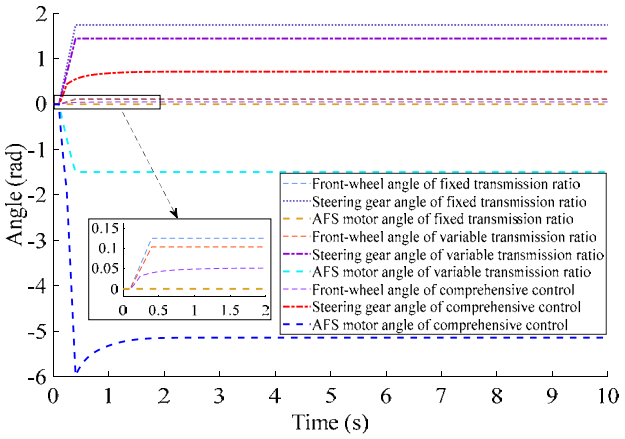

Table 8 The angle of mechanisms at stable

Control scheme	*Front wheel (rad)*	*Steering gear (rad)*	*AFS motor (rad)*
Fixed transmission ratio	0.1247	1.740	0
Variable transmission ratio control	0.1033	1.447	-1.493
Comprehensive control	0. 0512	0.717	-5.142

Based on Figure 22 and Table 8, the rotation direction for HW and AFS motor are opposite under VTR control and comprehensive control. Meanwhile, front wheel angle controlled by VTR control and comprehensive control is smaller than the fixed transmission ratio scheme. This indicates that the VTR control and comprehensive control play a certain role in maintaining steering stability of vehicle. Because of the limitation of the maximum steering transmission ratio, the additional angle from AFS motor controlled by VTR control is limited. For that, it is unable to provide a suitable AFS motor additional angle to maintain the steering stability. The comprehensive control breaks the constraint of maximum steering transmission ratio, and it allows the AFS motor to provide a larger additional angle. It

can make the actual state parameters of the vehicle better track the desired values.

5.3 Condition 3: hand-wheel sine input at high speed

The effectiveness of the comprehensive control strategy is further proved at high-speed with large HW angle inputs, the HW angle is set to a sine input as shown in Figure 23. The operating conditions of the vehicle are a high friction coefficient road with 0.85 and a constant speed of 100 km/h. Figure 24 displays the response of steering transmission ratio. Figure 25 shows the vehicle responses parameters under fixed transmission ratio, VTR control, and comprehensive control. Based on Figure 25, the maximum errors between the actual response parameters and the desired values under different control schemes occurs at the peak, and they are shown in Table 9. The angle responses of each steering mechanism are shown in Figure 26.

Figure 23 Hand-wheel angle for sine input (v = 100 km/h and μ = 0.85)

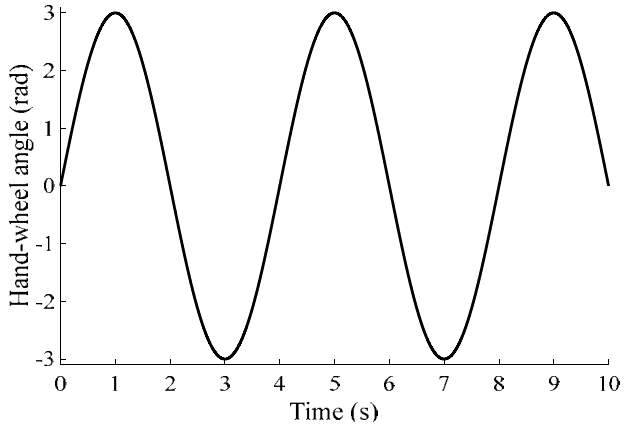

Figure 24 Transmission ratio response for sine input (v = 100 km/h, μ = 0.85) (see online version for colours)

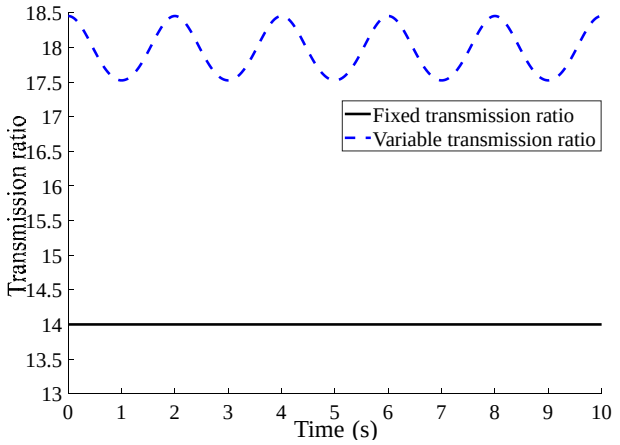

Figure 25 shows that the actual response parameters under comprehensive control can follow the desired value quickly and accurately. Figure 25(a) shows that the yaw rate under comprehensive control can effectively track the desired yaw rate, but the yaw rate of VTR control and fixed transmission ratio scheme fluctuates around the ideal value. Based on Table 9, the maximum errors e_r under fixed transmission ratio, VTR control, and comprehensive control are 0.3310 rad/s, 0.2883 rad/s and 0.0093 rad/s, respectively. As shown in Figure 25(b), the sideslip angle under comprehensive control is closer to the desired value. Based on Table 9, the maximum errors e_β under fixed transmission ratio, VTR control, and comprehensive control are 0.1373 rad, 0.1223 rad and 0.0356 rad, respectively. The results indicate that the comprehensive control can improve the stability of high-speed driving.

Figure 25 (a) The response curves of yaw rate (b) The response curves of sideslip angle responses (v = 100 km/h, μ = 0.85) (see online version for colours)

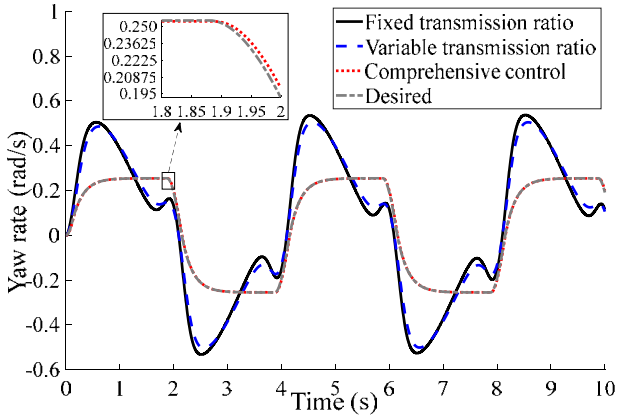

(a)

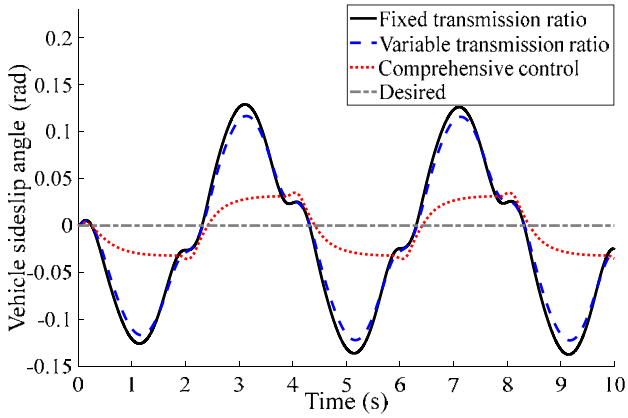

(b)

Table 9 The maximum values of e_γ and e_β at peak

Control scheme	e_γ *(rad/s)*	e_β *(rad)*
Fixed transmission ratio	0.3310	0.1373
Variable transmission ratio control	0.2883	0.1223
Comprehensive control	0.0093	0.0356

Figure 26 shows the phase difference between the HW angle and the AFS motor angle is approximately 180 degrees, and this makes the wheel angle under comprehensive control smaller than the wheel angle under

fixed transmission ratio. This can effectively improve driving stability at high speed.

Figure 26 The angle responses of each steering mechanism (v = 100 km/h, μ = 0.85) (see online version for colours)

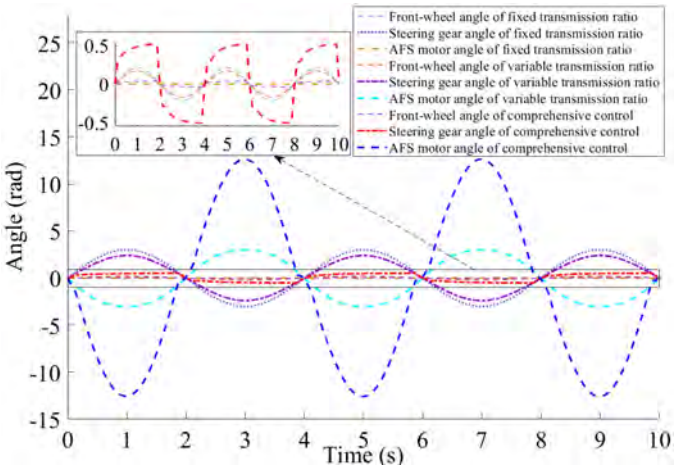

5.4 *Condition 4: double lane change at high-speed*

The DLC condition is adopted to verify the control strategy at vehicle speed 100km/h under fixed transmission ratio scheme, VTR control, and comprehensive control. Figure 27 shows the response of steering transmission ratio. The result of path tracking with different control schemes under DLC test is shown in Figure 28. Figure 29 displays the responses of vehicle sideslip angle and yaw rate. The maximum values of e_γ and e_β at peak are shown in Table 10. The angle responses of each steering mechanism are shown in Figure 30.

Figure 27 Transmission ratio response for DLC condition (v = 100 km/h, μ = 0.85) (see online version for colours)

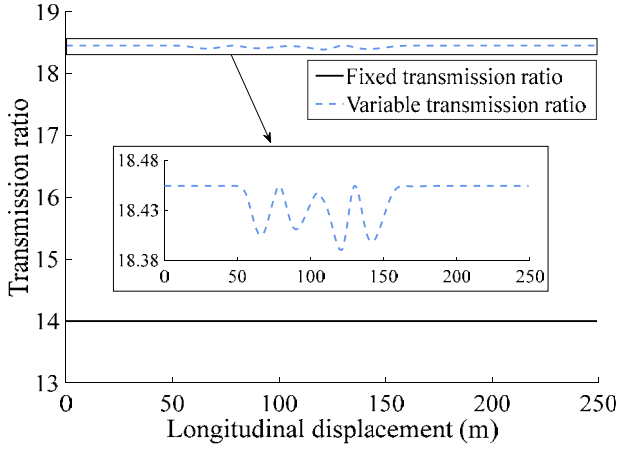

Figure 28 Driving trajectory under DLC condition (v = 100 km/h, μ = 0.85) (see online version for colours)

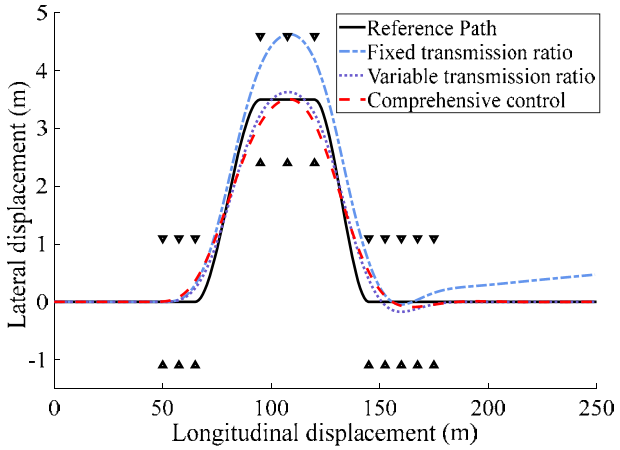

Figure 29 (a) Yaw rate responses (b) Vehicle sideslip angle responses (v = 100 km/h, μ = 0.85) (see online version for colours)

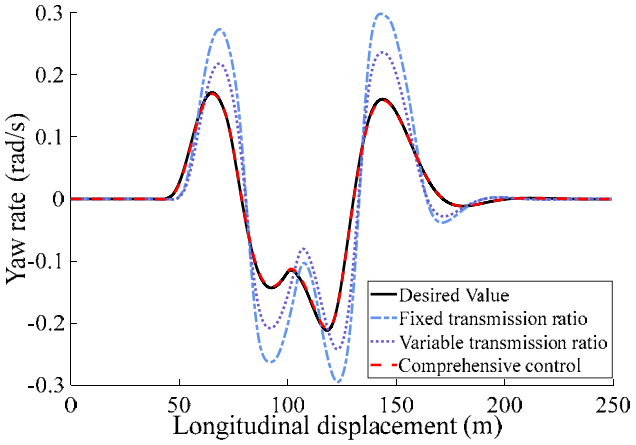

(a)

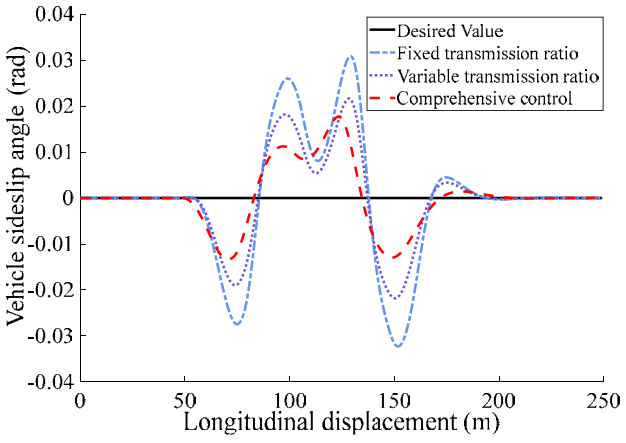

(b)

Figure 29(a) shows the yaw rate under the comprehensive control can track the desired value well, and the yaw rate under VTR control and fixed transmission ratio scheme has a large error with the desired value. In addition, compared to the vehicle with fixed transmission ratio characteristics, variable transmission control and comprehensive control can reduce the yaw rate effectively. As shown in Table 10, the maximum errors e_r under fixed transmission ratio, VTR control, and comprehensive control are 0.1766 rad/s, 0.1223 rad/s and 0.0037 rad/s, respectively. It is seen from Figure 29(b) that the sideslip angle under comprehensive control is closer to the desired value. Based on Table 10, the maximum errors e_β under fixed transmission ratio, VTR control, and comprehensive control are 0.0323 rad, 0.0218 rad and 0.0177 rad, respectively. The comprehensive control plays an important role in improving the stability of high-speed driving.

Figure 28 shows the vehicle trajectory under VTR control and comprehensive control can better track the ideal trajectory. The trajectory of vehicle with the fixed transmission ratio deviates significantly from the target trajectory.

Table 10 The maximum values of e_γ and e_β at peak

Control scheme	e_γ *(rad/s)*	e_β *(rad)*
Fixed transmission ratio	0.1766	0.0323
Variable transmission ratio control	0.1223	0.0218
Comprehensive control	0.0037	0.0177

Figure 30 shows that the rotation direction of AFS motor and HW for VTR control and comprehensive control is opposite. This can reduce actual front steering angle, and can improve the driving stability at the high speed effectively.

Figure 30 The angle responses of each steering mechanism (v = 100 km/h, μ = 0.85)

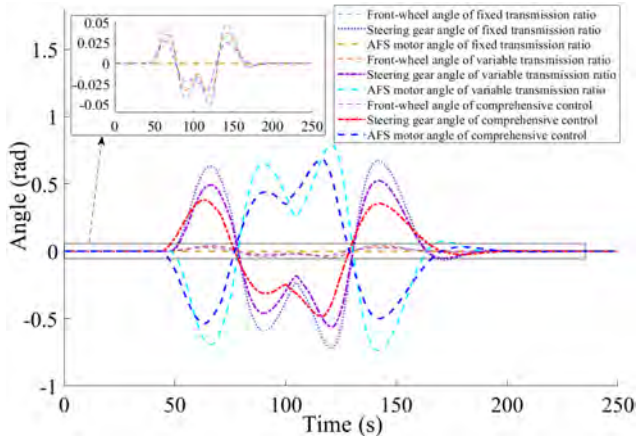

6 Conclusions

Based on the characteristic of AFS system, a comprehensive control strategy based on VTR and LQR is studied to enhance the vehicle handling performance. For avoiding the sudden change of hand-wheel torque effectively, the traditional VTR law is optimised based on the improved S-type function and PSO algorithm. In order to maintain the stability of the vehicle, the active steering control strategy is studied based on the optimised VTR law and LQR algorithm. The driver-vehicle verification platform is built, and the above strategies are verified by angular step, sine and double line change conditions. The results demonstrate that the comprehensive strategy can enhance tracking ability to the desired value effectively. It can reduce the deviation between the actual response parameters and the desired parameters. The comprehensive strategy can limit the maximum yaw rate effectively, and improve the steering stability with a large angle input at high speeds. The research can provide a theoretical basis for the design and development of AFS system.

The robustness of control systems is not discussed, and further research will focus on the robustness of control systems under disturbances such as the vehicle parameter uncertainty. This paper does not perform hardware-in-the-loop (HIL) verification of the control strategy, which will be a major future work. HIL verification for the control strategy is not performed, and this will be a major work in the future. The computational performance of PSO is not considered, and how to improve the performance of PSO algorithms will be concerned.

References

Cho, J. and Huh, K. (2019) 'Active front steering for driver's steering comfort and vehicle driving stability', *International Journal of Automotive Technology*, Vol. 20, No. 3, pp.589–596.

Choi, M. and Choi, S.B. (2016) 'MPC for vehicle lateral stability via differential braking and active front steering considering practical aspects', *Proceedings of the Institution of Mechanical Engineers, Part D: Journal of Automobile Engineering*, Vol. 230, No. 4, pp.459–469.

Ding, H., Guo, K., Li, F. and Zhang, J. (2010) 'A driver model for arbitrary road and speed following control based on acceleration feedback', *Journal of Mechanical Engineering*, Vol. 46, No. 10, pp.116–120+125.

Khajeh, A., Ghasemi, M.R. and Arab, H.G. (2019) 'Modified particle swarm optimization with novel population initialization', *Journal of Information and Optimization Sciences*, Vol. 40, No. 6, pp.1167–1179.

Kim, S.J., Kwak, B.H., Chung, S.J. and Kim, J.G. (2006) 'Development of an active front steering system', *International Journal of Automotive Technology*, Vol. 7, No. 3, pp.305–310.

Li, S., Wang, G., Guo, L., Li, Z., Lu, X., Yu, Z., Cui, G. and Zhang, J. (2018) 'NMPC-based yaw stability control by active front wheel steering', *IFAC-PapersOnLine*, Vol. 51, No. 31, pp.583–588.

Ma, L., Cheng, C., Guo, J., Shi, B., Ding, S. and Mei, K. (2023) 'Direct yaw-moment control of electric vehicles based on adaptive sliding mode', *Mathematical Biosciences and Engineering*, Vol. 20, No. 7, pp.13334–13355.

Pi, D., Yang, M., Liu, Y. and Liu, Y. (2021) 'Coordination strategy between AFS and ASB with fault-tolerant mechanism for ground vehicle', *Proceedings of the Institution of Mechanical Engineers, Part D: Journal of Automobile Engineering*, Vol. 235, No. 4, pp.1128–1148.

Qi, G., Fan, X. and Zhao, Z. (2021) 'Fuzzy and sliding mode variable structure control of vehicle active steering system', *Recent Patents on Mechanical Engineering*, Vol. 14, No. 2, pp.226–241.

Shimizu, Y., Kawai, T. and Yuzuriha, J. (1999) 'Improvement in driver-vehicle system performance by varying steering gain with vehicle speed and steering angle: VGS (variable gear-ratio steering system)', *SAE Transactions*, Vol. 108, No. 6, pp.630–639.

Song, J. (2016) 'Active front wheel steering model and controller for integrated dynamics control systems', *International Journal of Automotive Technology*, Vol. 17, No. 2, pp.265–272.

Ti, Y., Zheng, K., Zhao, W. and Song, T. (2022) 'A novel IMC-FOF design for four wheels steering systems of distributed drive electric vehicles', *Proceedings of the Institution of Mechanical Engineers, Part D: Journal of Automobile Engineering*, Vol. 236, No. 5, pp.842–856.

Wang, C., Deng, K., Zhao, W., Zhou, G. and Zhou, D. (2017) 'Stability control of steer by wire system based on μ synthesis robust control', *Science China Technological Sciences*, Vol. 60, No. 1, pp.16–26.

Wei, J., Shi, G. and Lin, Y. (2013) 'Design of new variable steering ratio for mechanical active steering system', *Proceedings of 2013 IEEE International Conference on Vehicular Electronics and Safety*, Dongguan, China, pp.27–30.

Wu, X. and Li, W. (2020) 'Variable steering ratio control of steer-by-wire vehicle to improve handling performance', *Proceedings of the Institution of Mechanical Engineers, Part D: Journal of Automobile Engineering*, Vol. 234, Nos. 2–3, pp.774–782.

Wu, X., Zhou, B., Wu, T. and Pan, Q. (2022) 'Research on intervention criterion and stability coordinated control of AFS and DYC', *International Journal of Vehicle Design*, Vol. 90, Nos. 1–4, pp.116–141.

Zhang, J., Li, X. and Li, J. (2022) 'Design of variable ratio mathematical model for steer-by-wire system', *International Journal of Vehicle Performance*, Vol. 8, No. 4, pp.387–404.

Zhao, B., Fan X. and Qi, G. (2022) 'Variable transmission ratio and active steering control for steer-by-wire steering', *International Journal of Vehicle Systems Modelling and Testing*, Vol. 16, No. 4, pp.290–312.

Zhao, J., Wang, X., Liu, T., Liang, Z., Hua, X. and Wang, Y. (2021) 'Hierarchical control for cornering stability of dual-motor RWD vehicles with electronic differential system using PSO optimized SOSMC method', *Advanced Engineering Informatics*, Vol. 50, No. 1, p.101413.